Performance Improvement of Variable Speed Rotors by Gurney Flaps

Dong Han*[1], **Chen Dong[1]**, and **George N. Barakos[2]**

[1]National Key Laboratory of Science and Technology on Rotorcraft Aeromechanics, Nanjing University of Aeronautics and Astronautics, Nanjing 210016, China

[2]CFD Laboratory, School of Engineering, James Watt South Building, University of Glasgow, Glasgow G12 8QQ, Scotland, UK

Gurney flaps are used for improving the performance of variable speed rotors. An analytical model able to predict helicopter rotor power is first presented, and the flight data of the UH-60A helicopter is used for validation. The predictions of the rotor power are in good agreement with the flight test data, justifying the use of this tool in analyzing helicopter performance. A fixed Gurney flap can enhance the performance of variable speed rotors and expand the corresponding flight envelop, especially near stall and high speed flight. A retractable Gurney flap at 1/rev yields more power savings than a fixed Gurney flap or a retractable one with **a higher** harmonic prescribed motion. At a speed of 200km/h, the retractable Gurney flap, actuated at 1/rev, can obtain 3.22% more power reduction at a rotor speed of 85% nominal rotor speed, and this value is 8.37% at a speed of 220km/h. The height corresponding to the minimum power increases slowly in low to medium speed flight, and increases dramatically in high speed flight. With increasing take-off weight (i.e. rotor thrust), the retractable Gurney flap at 1/rev can obtain more rotor power savings.

Keywords: Performance; Variable Speed Rotor; Gurney Flap; Harmonic Motion

1. Introduction

Reducing rotor speed in hover and forward flight, has been extensively investigated to save helicopter power and improve helicopter performance [1-9]. Kang et al. analyzed several rotor morphing concepts, and the comparisons showed that a reduced rotor speed could yield more power savings than other investigated concepts [10]. Varying rotor speed, primarily changes the rotor profile power. At high thrust and/or high speed, the rotor induced power and/or fuselage parasitic power dominate the helicopter power. The potential of the variable rotor speed in decreasing rotor power diminishes significantly in these flight states [6, 8].

The Gurney Flap (GF) is a lift enhancement device, invented by the race car driver Dan Gurney in 1960s [11]. GF attracted much attention not only due to its efficiency and simplicity, but also due to its lower power consumption than a plain-flap configuration[12]. It has been extensively explored to improve helicopter rotor performance. The investigations by Kentfield indicated that GFs could enhance helicopter rotor performance under many circumstances [13], which is primarily due to the increase of the maximum lift coefficient, and lift-to-drag ratio in the retreating side of rotor blades. Kinzel et al. utilized deployable GFs (Miniature Trailing-Edge Effectors, MiTEs) to obtain helicopter power savings [14]. The analysis showed that MiTEs were most effective for increasing performance at high altitude, large payloads, high flight speeds, or any combination of these, which is because of their better performance near stall. Pastrikakis et al. investigated the potential effect of a GF on the performance of W3 Sokol blade in hover and forward flight [15, 16]. The results showed an increase in the aerodynamic performance by GFs, especially for high thrust conditions. GFs can also be utilized to reduce vibrations in helicopter rotors. Min et al. calculated the performance of a rotor equipped with a GF in forward flight, and descent using a hybrid Navier-Stokes/free-wake solver [17]. Their investigations indicated that GFs had the potential to reduce rotor vibratory loads, and the GF with fixed height could decrease the descent rate needed to maintain autorotation. Liu et al. used microflaps (deployable GFs) for vibration

reduction [18]. Their open-loop phase-sweep studies showed more than 80% 4/rev vertical shear reduction at high-vibration BVI (blade vertex interaction) flight conditions, and the closed-loop control analysis showed over 90% reduction in the combined vibration objective function. Min et al. used a dynamically deployed GF to conduct rotor vibration control [19]. The CFD-CSD (Computational Fluid Dynamics - Computational Structural Dynamics) coupled analysis showed that more than 80% of the 4/rev vertical vibratory hub loads could be reduced with an optimized GF schedule, and the individual control of multiple segments of flaps along the blade span could be used to conduct multiple signal controls. It is obvious that GF can be used to improve helicopter rotor performance, especially in high thrust, high speed and/or high altitude, and may simultaneously reduce rotor vibratory loads.

With decreasing rotor speed, helicopter rotors have to increase their blade pitch angles to maintain balance due to the decrease of the dynamic pressure. This enlarges the stall area, and decreases the power savings obtained by the reduced rotor speed. To compensate this reduction of performance improvement, retractable GFs of variable height are utilized to improve the performance of variable speed rotors. A helicopter rotor power prediction model, which includes a blade model, aerofoil table look-up method, the Pitt-Peters inflow model [20], a fuselage model, and a propulsive trim method [21], is used here. The flight data of the UH-60A helicopter [22] is utilized to validate the model. Parametric analyses of different retractable GFs were investigated with the validated model to explore how much power savings can be achieved further based on the power reduced by variable rotor speed.

2. Modeling and Validation

To determine the optimal parameters of the GF for minimum rotor power, a parameter sweep for each flight state is conducted. This process has to be repeated for several rotor power settings. If a single computation requires one minute of CPU time, to find the minimum power can span dozens of hours. Since the objective of this work is to explore the potential of GF in reducing the power of variable speed rotors, an analytical model to predict the helicopter rotor power is used. This model estimates the rotor power within less than a second using a standard personal computer.

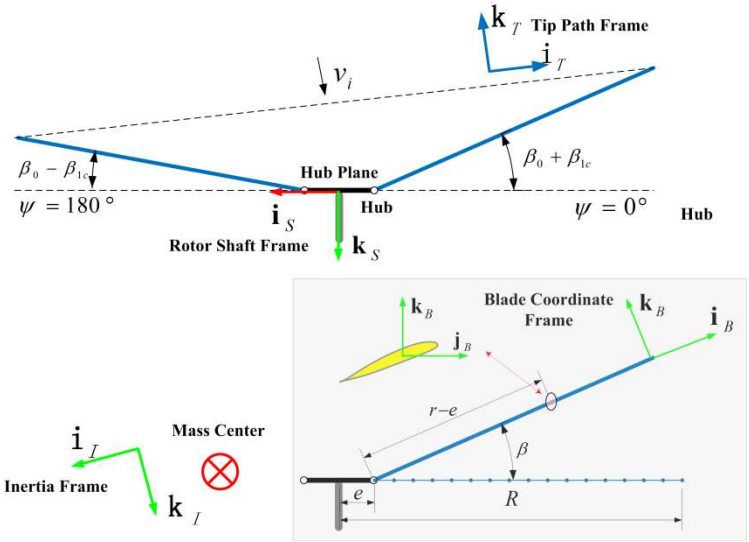

Figure 1 Coordinate frames.

The blade model is based on a rigid beam with a hinge offset and a hinge spring, used to match the fundamental flapwise blade frequency. For the analysis of the performance of variable speed rotors, using a rigid blade model and omitting the change of blade twist were indubitably acceptable [6]. GFs attached to rotor blades not only change the lift

and drag coefficients, but also the moment coefficients. This can introduce a change of blade twist. Since advanced helicopters with variable speed rotors, such as the X2 and A160, usually adopt rigid rotors, their higher torsional stiffness can significantly reduce the change amplitude of blade twist. The inability in predicting the influence of the change of blade twist on the performance, lowers the prediction precision. However, it still renders acceptable for predictions for rotor performance analysis and comparative studies [14, 23, 24].

The position of an arbitrary point on the pitch axis in the rotor shaft coordinate system as shown in Figure 1 can be expressed as

$$\begin{cases} r_x = -e\cos\psi - (r-e)\cos\beta\cos\psi \\ r_y = e\sin\psi + (r-e)\cos\beta\sin\psi \\ r_z = -(r-e)\sin\beta \end{cases},$$

(1)

where, r is the radial coordinate of the point, ψ is the azimuth angle, β is the blade flapping angle, and e is the flap hinge offset. The velocity vector, in the blade airfoil frame, of this point with respect to the local airflow has three components: the motion by the blade flapping and rotation, the forward speed of the helicopter and the rotor induced velocity. This can be expressed as

$$\begin{Bmatrix} U_R \\ U_T \\ U_P \end{Bmatrix} = [T_{BS}]\left[\begin{Bmatrix} \dot{r}_x \\ \dot{r}_y \\ \dot{r}_z \end{Bmatrix} - [T_{SI}]\begin{Bmatrix} V_x \\ V_y \\ V_z \end{Bmatrix} - [T_{ST}]\begin{Bmatrix} 0 \\ 0 \\ v_i \end{Bmatrix}\right],$$

(2)

where, $\dot{r}_x$, $\dot{r}_y$ and $\dot{r}_z$ are the velocity components in the rotor shaft coordinate system of the arbitrary point on the pitch axis. V_x, V_y and V_z are the components of local air velocity in the inertia frame. v_i is the induced velocity. $[T_{BS}]$ denotes the transformation matrix from the rotor shaft frame to the blade airfoil frame. $[T_{ST}]$ denotes the transfomation matrix from the rotor tip path plane to the rotor shaft frame. $[T_{SI}]$ denotes the transformation matrix from the inertial frame to the rotor shaft frame, as shown in Figure 1. The induced velocity over the rotor disk is predicted by the Pitt-Peters inflow model [20], which captures the first harmonic variation of induced velocity in azimuth as following

$$\frac{v_i}{\Omega R} = \lambda_0 + \lambda_c \frac{r}{R} cos\psi + \lambda_s \frac{r}{R} sin\psi,$$

(3)

where, Ω is the rotor speed, R is the rotor radius, and λ is the rotor inflow ratio. The angle of attack and the resultant velocity are derived from the velocity vector of Equation 2 as

$$\alpha = \theta_0 + \theta_{1c}\cos\psi + \theta_{1s}\sin\psi + \theta_{tw}(r) - \arctan\left(\frac{U_P}{U_T}\right),$$

(4)

$$U_B = \sqrt{U_P^2 + U_T^2},$$

(5)

where, θ_0, θ_{1c}, and θ_{1s} are the collective pitch, lateral cyclic pitch and longitudinal pitch. θ_{tw} is the local pretwist angle as a function of the radial coordinate r. Look-up table aerofoil aerodynamics is used to calculate the lift $C_l(\alpha, M_a)$ and drag coefficients $C_d(\alpha, M_a)$ of the blade elements according to the local resultant air flow and angle of attack. M_a is the Mach number at the point r, which can be calculated as U_B/a with a as the sonic velocity.

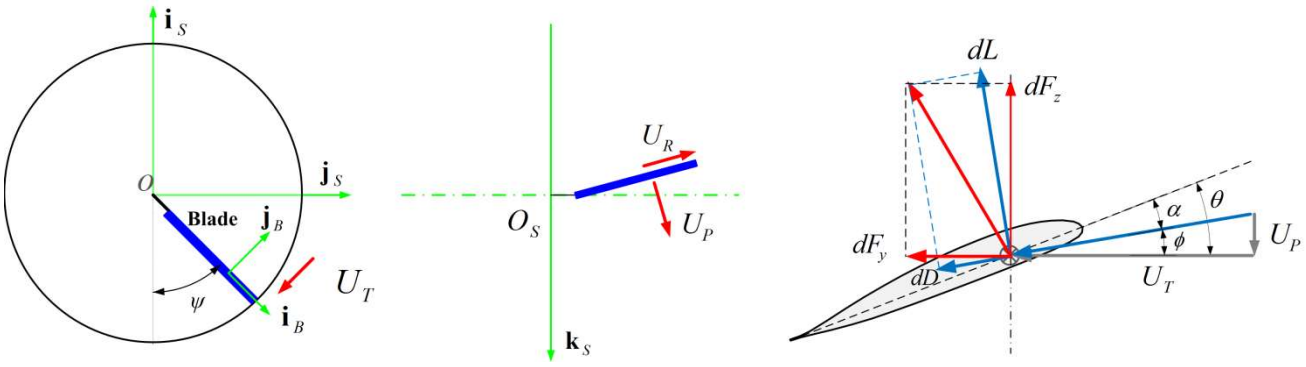

Figure 2 Velocities and forces on an airfoil segment.

The aerodynamic forces on the corresponding airfoil segment shown in Figure 2 are

$$\begin{cases} dL = \frac{1}{2}\rho U_B^2 c C_l dr \\ dD = \frac{1}{2}\rho U_B^2 c C_d dr \end{cases}, \tag{6}$$

where, ρ is the air density, and c is the chord length of the blade. The aerodynamic forces are then transferred to the blade coordinate frame, as shown in Figure 2 and are given by

$$\begin{cases} dF_x = 0 \\ dF_y = -(dL\sin\phi + dD\cos\phi) \\ dF_z = dL\cos\phi - dD\sin\phi \end{cases}. \tag{7}$$

Taking into account the inertial force, the resultant forces on the blade segment, in the rotor shaft frame of reference are

$$\begin{Bmatrix} {}^S dF_x \\ {}^S dF_y \\ {}^S dF_z \end{Bmatrix} = [T_{SB}] \begin{Bmatrix} dF_x - m\ddot{r}_x dr \\ dF_y - m\ddot{r}_y dr \\ dF_z - m\ddot{r}_z dr \end{Bmatrix}, \tag{8}$$

where, $[T_{SB}] = [T_{BS}]^{\mathrm{T}}$. The hub forces and moments of the main rotor are derived from the resultant root forces and moments of the blades

$$\begin{cases} F_{Hx} = \frac{N_b}{2\pi}\int_0^{2\pi}\int_e^R {}^S dF_x \, d\psi \\ F_{Hy} = \frac{N_b}{2\pi}\int_0^{2\pi}\int_e^R {}^S dF_y \, d\psi \\ F_{Hz} = \frac{N_b}{2\pi}\int_0^{2\pi}\int_e^R {}^S dF_z \, d\psi \end{cases}, \tag{9}$$

where, N_b is the number of blades. Similarly, the roll and pitch moments of the rotor are

$$\begin{cases} M_x = \frac{N_b}{2\pi}\int_0^{2\pi}[e\,{}^S F_z - k_\beta(\beta - \beta_P)]\sin\psi d\psi \\ M_y = \frac{N_b}{2\pi}\int_0^{2\pi}[e\,{}^S F_z - k_\beta(\beta - \beta_P)]\cos\psi \, d\psi \end{cases}, \tag{10}$$

where, k_β is the stiffness of the hinge spring, and β_P is the blade procone angle. The rotor torque can be derived as

$$Q = \frac{N_b}{2\pi}\int_0^{2\pi}\int_e^R [e + (r - e)\cos\beta] dF_y \, d\psi.$$

(11)

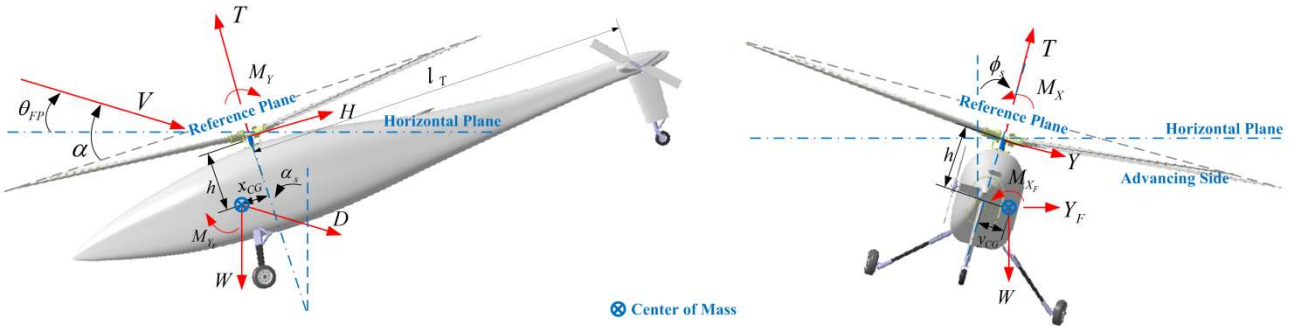

Figure 3 Forces and moments on a helicopter.

The fuselage is treated as a rigid body with specified aerodynamic forces and moments. For simplicity, the thrust of the tail rotor is determined by the main rotor torque, divided by the distance between the hub center of the tail rotor and the main rotor shaft. The power and collective pitch of the tail rotor are determined by the blade element theory with uniform inflow.

Given three pitch controls (collective and two cyclics) and two rotor shaft attitude angles (longitudinal and lateral tilts), the periodic response of the rotor in steady forward flight can be obtained for a prescribed forward speed. The hub forces and moments of the main rotor are balanced by the forces and moments acting on the fuselage and tail rotor. The forces and moments on the fuselage are determined by the flight state and attitude angles. The thrust and power of the tail rotor are derived from the rotor **torque** and flight state. These force and moment components, as shown in Figure 3, constitute the equilibrium equations of the helicopter

$$\begin{cases} T - W = 0 \\ D + H - T\alpha_s = 0 \\ Y + Y_F + T\phi_s = 0 \\ M_Y + M_{Y_F} + W(h\alpha_s - x_{CG}) - hD = 0 \\ M_X + M_{X_F} + W(h\phi_s - y_{CG}) + hY_F = 0 \end{cases}, \tag{12}$$

where, T, H, Y, M_Y and M_X are the rotor thrust, drag force, side force, pitching moment and roll moment; D, Y_F, M_{Y_F} and M_{X_F} are the fuselage drag, side force, pitching moment, and roll moment; W is the helicopter weight; x_{CG}, y_{CG} and h are the longitudinal, lateral and vertical distance from the mass center of the helicopter to the rotor hub center; α_s and ϕ_s are the longitudinal and lateral tilt angles of the rotor shaft. The equations are solved to update the pitch controls and rotor attitude angles for the next iteration. After several iterations of the periodic rotor responses and solutions of the equilibrium equations, the converged or trimmed pitch controls and rotor attitude angles can be obtained. Then, the main rotor power and related information of the helicopter can be derived. **The flowchart of the performance prediction method is shown in Figure 4.**

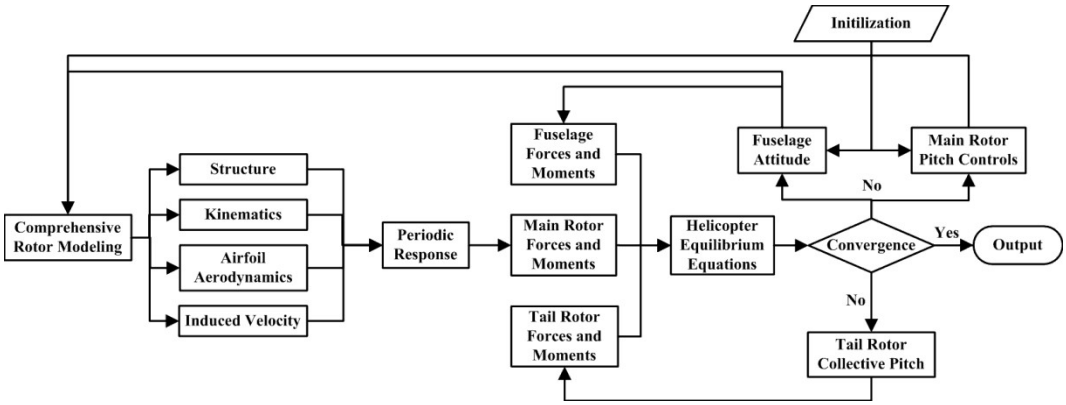

Figure 4 Flowchart of performance prediction.

The flight test data of the UH-60A helicopter [22] is utilized to validate the model used in this work. The parameters of the main and tail rotors are listed in Tables 1 and 2 [25-28]. For the performance analysis, only the aerodynamic drag force is considered in the fuselage model. The fuselage drag equation utilized in the present analysis is [22]

$$\frac{D}{q}\,(\mathrm{ft}^2) = 35.83 + 0.016 \times (1.66\alpha_s^2), \tag{13}$$

where, D is the fuselage drag, q is the dynamic pressure, and α_s is the aircraft pitch angle. The distance from the hub center of tail rotor to the rotor shaft is 9.93 m. The vertical distance from the mass center of the helicopter to the rotor hub is 1.78 m. The comparisons of the prediction of the rotor power with the flight test data for the takeoff weight coefficients 0.0065, 0.0074, 0.0083 and 0.0091 are shown in Figure 5. It is obvious that the predictions by the present method are generally in good agreement with the flight test data for the weights considered. This justifies the use of present method for the analysis of helicopter performance. This model has also been utilized to analyze the effect of dynamic blade twist on rotor performance [29]. **The difference in the case of $C_w = 0.0083$ between the advance ratios 0.1 and 0.2 is a little larger, which may be due to some unaccounted factors, such as aerodynamic interactions, transient wind, local temperature, working state of the test instrument and so on.**

Table 1: Main rotor parameters

Main Rotor Radius	8.18m
Main Rotor Speed (100%)	27.0 rad/s
Blade Chord Length	0.527m
Blade Twist	Nonlinear
Blade Airfoil	SC1095/SC1094R8
Number of Blades	4
Flap Hinge Offset	0.381 m
Blade Mass per Unit Length	13.9 kg/m
Longitudinal Shaft Tilt	3°

Table 2: Tail rotor parameters

Tail Rotor Radius	1.68 m
Tail Rotor Blade Chord	0.247 m

Tail Rotor Speed	124.6 rad/s
Tail Rotor Blade Twist	-18°
Blade Airfoil	NACA0012
Number of Blades	4

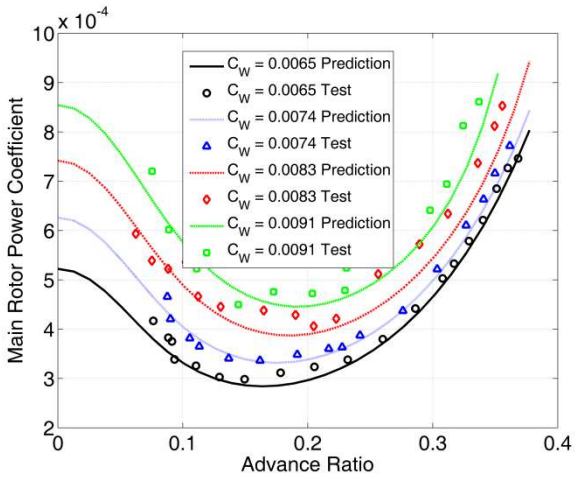

Figure 5 Comparison of predictions with flight test data.

The methodology of Ref. 13 for capturing the change of the aerodynamic characteristics of NACA 0012 airfoil with a GF is utilized here. For the NACA0012 airfoil with a GF within the height ratio range $0 \le d/c \le 5\%$ [13], the lift and drag coefficients C_l and C_d can be written as

$$C_l = C_l^0 + \Delta C_l, \tag{14}$$

$$C_d = C_d^0 + 0.135 C_d^{0\,-\frac{1}{3}} \left(\frac{d}{c}\right)^{\frac{4}{3}}, \tag{15}$$

$$\Delta C_l = 0.31858\left(\frac{d}{c}\times 100\right) - 0.07281\left(\frac{d}{c}\times 100\right)^2 + 0.00693\left(\frac{d}{c}\times 100\right)^3, \tag{16}$$

where, d is the height of GF, c the chord length, C_l^0 and C_d^0 the lift and drag coefficients without GF. The parameters of the GF are shown in Figure 6. For a retractable GF, the mounting angle β is 90°, and the height is given as a prescribed value.

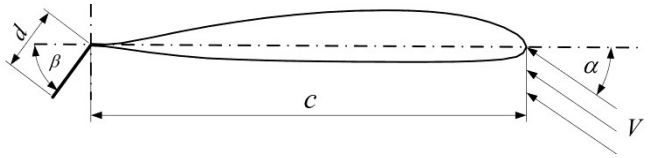

Figure 6 Configuration of a GF.

The comparisons of the lift coefficients between the test data in Ref. 30 and the prediction based on the C81 airfoil table are shown in Figure 7, which shows the prediction is generally in good agreement with the test data. In the following analysis, the rotor blade airfoil is changed to the airfoil NACA 0012. In the following analysis, the maximum

height ratio d/c is limited to be less than 5.0% and the GF extends from 70% to 90% of the rotor radius.

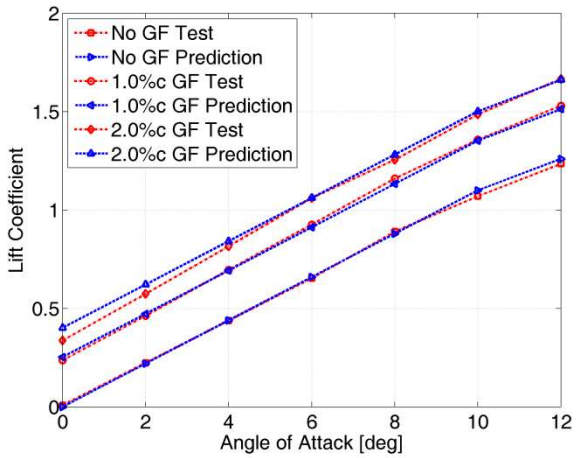

Figure 7 Comparison between test and prediction data.

The power reduction ratio is defined to determine the benefit in rotor power savings as

$$\eta = (1 - P/P_b) \times 100\%, \tag{17}$$

where, P is the rotor power to be compared with, and P_b is the baseline rotor power. The baseline power is defined as the rotor power at sea level at 100%Ω and without any GF. In the following analysis, the baseline weight is 8322.3kg, and the corresponding weight coefficient at 100%Ω is 0.0065.

3. GF with Fixed Height

For different rotor speeds and GF heights, the helicopter rotor power is shown in Figure 8. The power for the fixed-height GF has a minimum for heights ranging $0 \le d/c \le 5\%$. To determine the minimum power, a parameter sweep with 0.1% increment of height ratio at a prescribed forward flight speed is conducted. With decreasing rotor speed, the rotor power generally decreases. On the other hand, the rotor power at 85%Ω is larger than the value at 90%Ω, when the forward speed is larger than 240 km/h. So, for high speed forward flight, an excessive decrease of the rotor speed is not necessary. Compared with the clean blade, the power with GF decreases by 3.67, 6.67, 14.2 and 30.6 kW, at a forward speed of 200 km/h and rotor speeds of 100%, 95%, 90% and 85%, respectively. It is obvious that, at lower rotor speeds, larger power savings can be obtained, and the GF can enhance the performance of variable speed rotors.

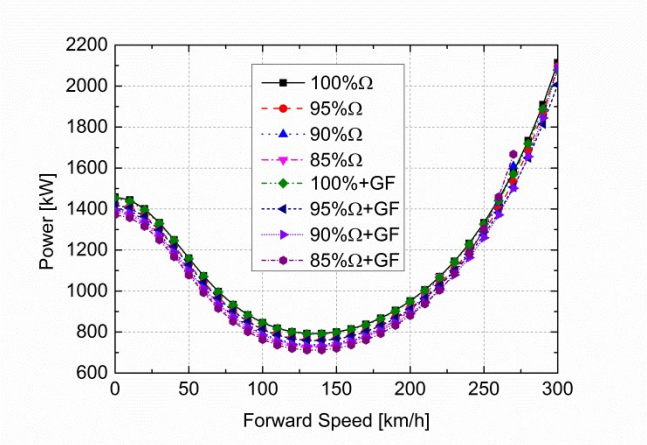

Figure 8 Helicopter power for different rotor speeds and GF heights.

The corresponding power reductions are shown in Figure 9. At full rotor speed, the rotor power with the GF decreases by 0.499% in hover, and varies smoothly with flight speed. At a speed of 250 km/h, the reduction begins to increase distinctly with forward speed, and touches the maximum value 1.66% at a speed of 300 km/h. The GF exhibits better performance at high speed flight. For rotor speeds of 95%Ω, 90%Ω, and 85%Ω, the power reduction increases first and then decreases. With decreasing rotor speed, the attainable maximum forward speed decreases. When the rotor speed is reduced to 85%Ω, the helicopter cannot fly faster than 220 km/h. With the GF, the maximum speed extends to 270 km/h. At a rotor speed of 90%Ω, the difference between the power reductions with and without GF is 0.63%, 0.67%, 1.49%, 2.92% and 6.77% at 0, 100, 200, 250, and 270 km/h, respectively. Since the GF does not change the blade tip Mach number, the better airfoil performance with the GF, especially near stall, is responsible for the power reduction. It is obvious that the GF can enhance the performance of variable speed rotors and expand the corresponding flight envelop, especially near stall and a high speed flight.

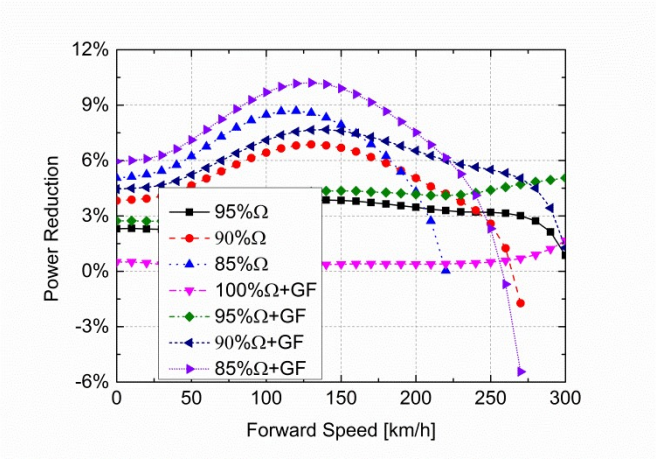

Figure 9 Power reduction for different rotor speeds and GF heights.

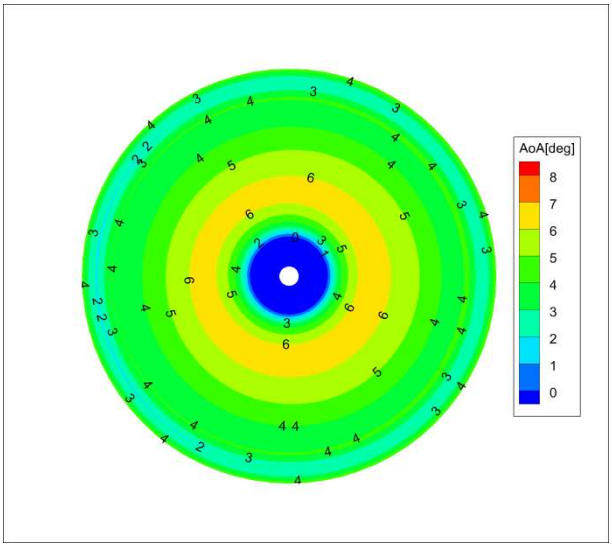

Figure 10 Distribution of angle of attack in hover.

The reduction of the rotor power in hover may appear, since the GF usually works best at high pitch angles. The distribution of the angle of attack in hover is shown in Figure 10. Within the region between 70%R-90%R, the angle of attack is between 4º to 6º. For these angles, a suitable height of GF (less than 1%c) can increase the lift to drag ratio, as shown in Figure 6 in Ref. 13. That is the reason why the power can be reduced in hover. With the decrease in the rotor speed, the angle of attack increases, and the GF benefit increases naturally.

The GF heights corresponding to minimum power are shown in Figure 11. With the forward speed, the height first decreases slightly, and then increases. At high speed flight, it increases dramatically. With decreasing rotor speed, the required GF height increases. At a speed of 260 km/h and rotor speed of 85%Ω, the height ratio is 5.0%. It can therefore be anticipated that, larger maximum forward speed can be obtained with larger GF height.

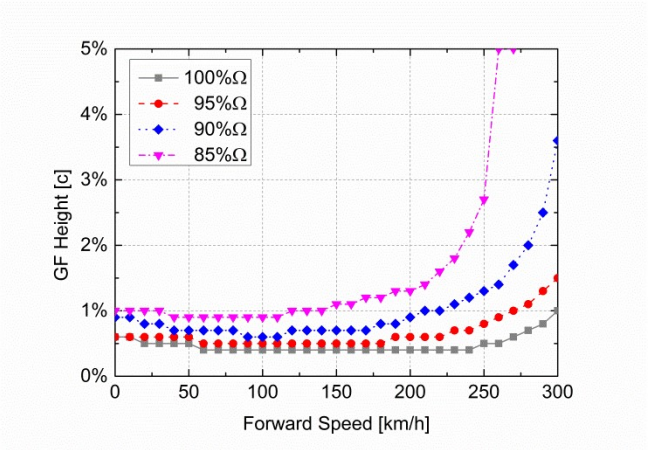

Figure 11 GF height corresponding to minimum power.

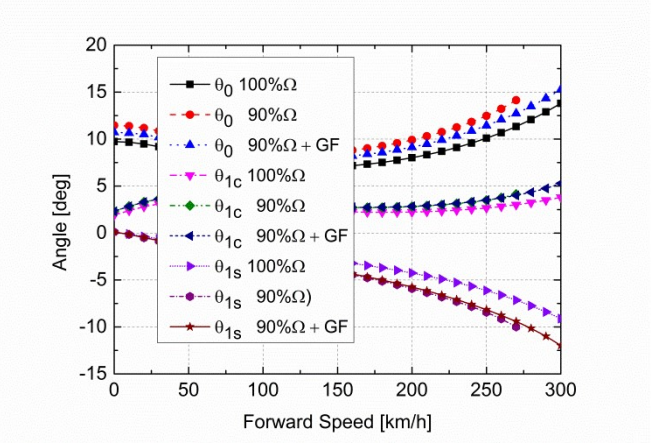

Figure 12 The collective, longitudinal and lateral cyclic pitches for the fixed height GF.

The collective pitch θ_0, longitudinal cyclic pitch θ_{1c}, and lateral cyclic pitch θ_{1s} at a rotor speed of 90%Ω with and without GF compared with the values at 100%Ω are shown in Figure 12. With decreasing rotor speed, the absolute values of the collective and cyclic pitches increase. The decrease of the dynamic pressure results in increased pitch angles to maintain balance of the helicopter. These trends are similar as those in Ref. 31. The deployment of the GF decreases θ_0, and the magnitude is relatively small. The θ_{1c} and θ_{1s} changes slightly. The longitudinal tilt angle α_s and lateral tilt angle ϕ_s of rotor shaft are shown in Figure 13. α_s and ϕ_s decrease with decreasing rotor speed, which have the same trend as those in Ref. 31. α_s and ϕ_s change little compared with the values without the GF. It is obvious that the

GF primarily changes θ_0, which is due to the lift enhancement effect.

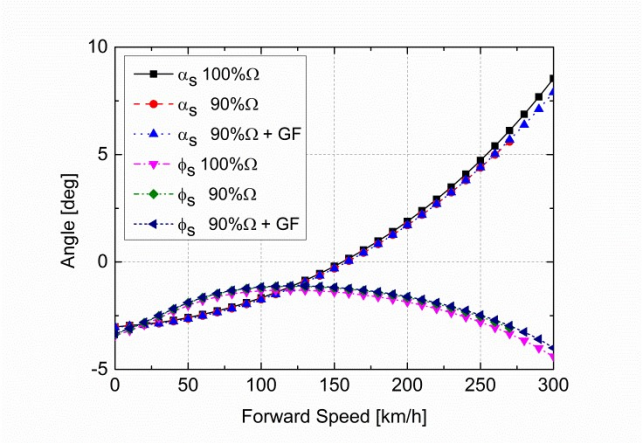

Figure 13 The longitudinal and lateral tilts of rotor shaft for the fixed height GF.

4. Retractable GF

In the following analysis, the GF height is prescribed as

$$h = A[1 + sin(n\Omega t + \phi)], \tag{18}$$

where, A is the average GF height, n is the harmonic number, Ω is the rotor speed, and ϕ is the phase of harmonic motion.

4.1 1/rev

Figure 14 shows the rotor power for different forward speeds and phases of the 1/rev harmonic motion of the GF. The amplitude of the GF motion is set to 2%c. At low speed flight, the change of the rotor power with the flap phase is substantially small. At high speed flight, the power changes distinctly. At a speed of 300km/h, and at 340° phase, the power increases by 3.99%. As the phase shifts to 180°, the power decreases by 3.51%. The phase of the GF motion has a significant influence on the rotor power. The phases corresponding to the minimum power for the investigated speeds are around 180°. In the following analyses related to the 1/rev GF motion, the phase is set to 180°.

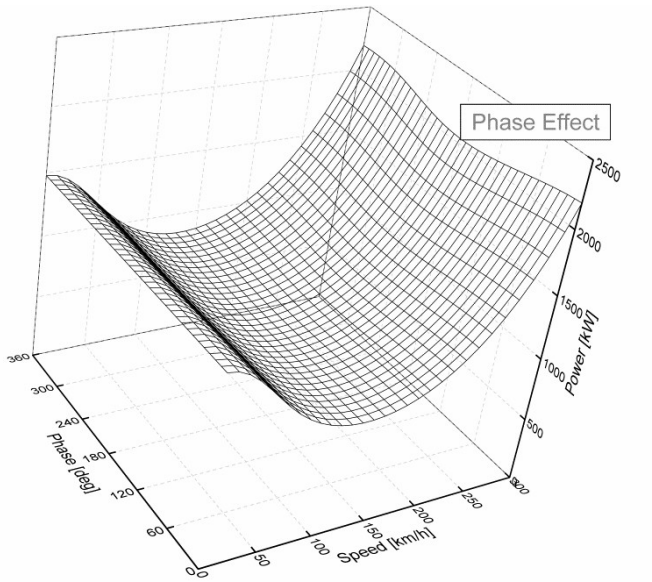

Figure 14 Rotor power for different forward speed and the phase of GF (2%c).

Figure 15 shows the power reduction for different rotor speeds. Compared to the fixed GF height, the 1/rev retractable GF yields the larger power reduction. At a speed of 300 km/h and rotor speed of 100%Ω, the maximum power reduction is 3.51%. This value is 1.66% for the fixed height GF. As the rotor speed decreases by 5%, the two values became 7.63% and 5.06%. With increasing forward speed, the difference between the power reduction with and without the GF increases, especially for high speed flight. At a speed of 200 km/h, the differences at speeds of 95%Ω, 90%Ω and 85%Ω are 0.70%, 1.49% and 3.22%, respectively. At 220 km/h and 85%Ω, the difference is 8.37%, which is much larger than the value at the speed of 200km/h. It is obvious that the GF can achieve better performance improvement in lower rotor speeds and higher speed flight, which indicates that the GF is more effective at high thrust and speed. The maximum forward speed can be attained by deploying the GF, highlighting its potential in expanding the flight envelope of helicopters.

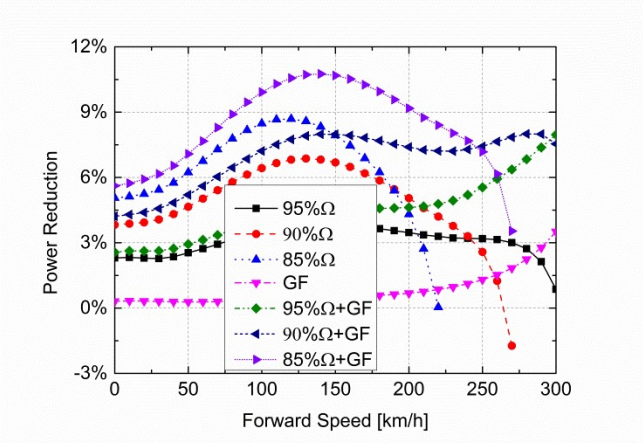

Figure 15 Power reduction for the 1/rev motion.

Figure 16 compares of the distributions of the angle of attack for different rotor speeds and GF heights at a flight speed of 200 km/h. Reducing the rotor speed (90%Ω), the overall angle of attack increases to provide enough thrust and maintain balance. The angle of attack in the retreating side increases distinctly. The region with larger than 10° of angle

of attack expands, and a region with 11° emerges. This also indicates the deterioration of rotor loads. With the GF, the average angle of attack decreases, which is due to the lift enhancement by the GF. The radial distribution of the angle of attack becomes less abrupt, which indicates alleviation of rotor loads.

Figure 17 shows the GF height corresponding to the minimum rotor power at the prescribed rotor and forward speeds. With increasing forward speed, the GF height increases. The trend changes smoothly at low to medium speeds. For high speed flight, the required height increases dramatically. Reducing the rotor speed, larger height is needed. At high forward speed, a GF larger than 2.5%c is needed, which indicates that the maximum forward speed can be extended if a larger GF is available.

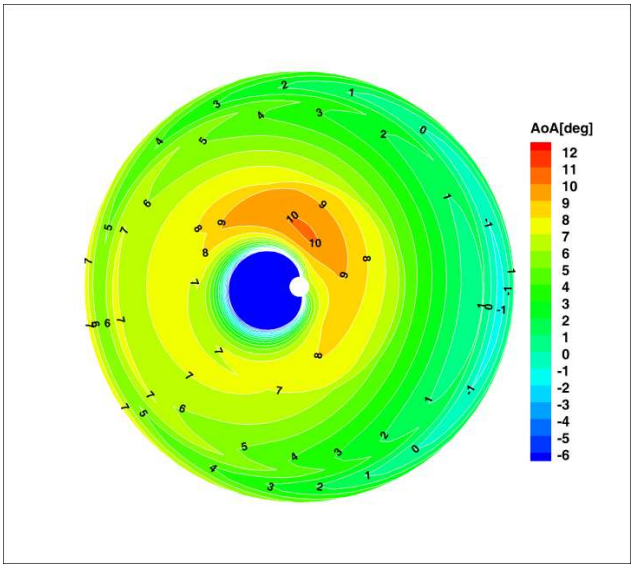

(a) 100%Ω and $A = 0$

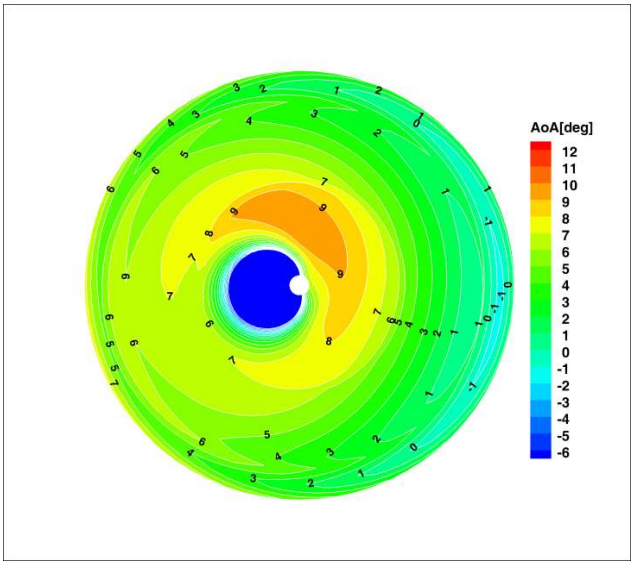

(b) 100%Ω and $A = 2\%c$

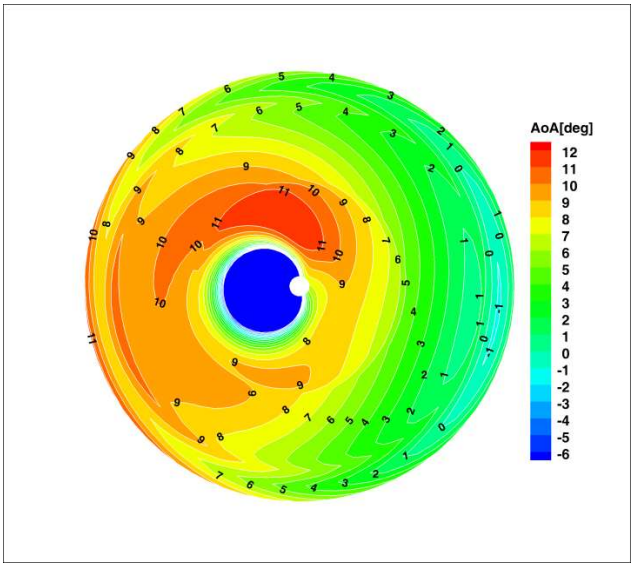

(a) 90%Ω with $A = 0$

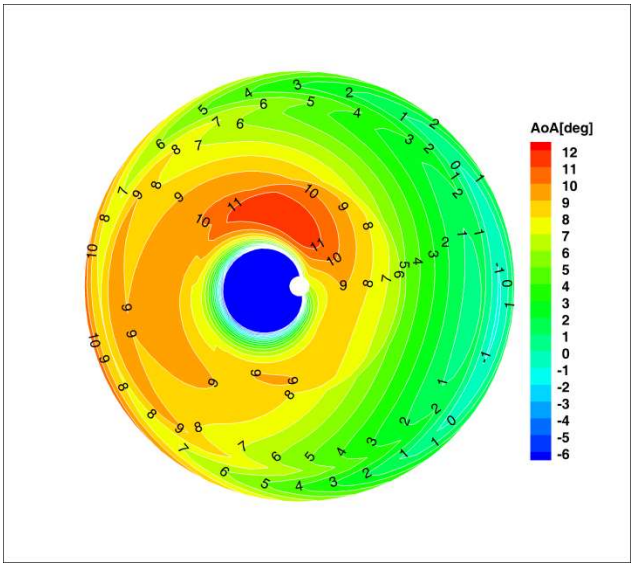

(b) 90%Ω and $A = 2\%c$

Figure 16 Distribution of the angle of attack at a flight speed of 200km/h.

The collective pitch θ_0, longitudinal cyclic pitch θ_{1c}, and lateral cyclic pitch θ_{1s} at a rotor speed of 90%Ω with and without the 1/rev GF are compared with the values at 100%Ω are shown in Figure 18. The trends are similar as those of the fixed height GF. The deployment of the 1/rev GF decreases θ_0, and its magnitude is a slightly larger than the fixed

height GF. θ_0 deceases by 1.04° for the fixed height GF, and this value is 1.46° for the 1/rev GF at a speed of 250 km/h and rotor speed of 90%Ω. The θ_{1c} and θ_{1s} change substantially small. Compared with the fixed height GF, θ_{1s} decreases larger. The longitudinal tilt angle α_s and lateral tilt angle ϕ_s of rotor shaft are shown in Figure 19, which changes little compared with the values without the deployment of GF.

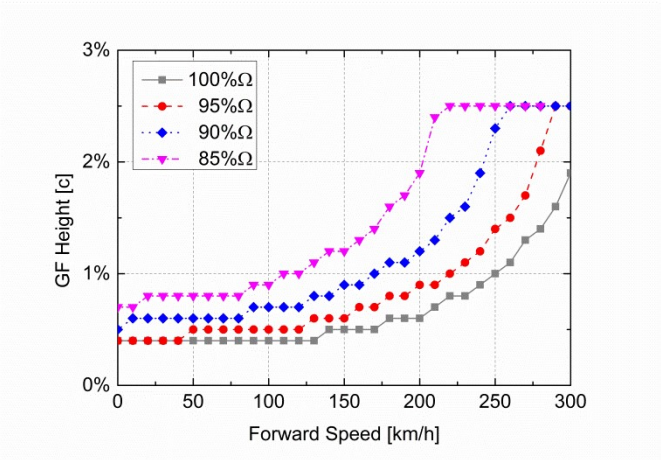

Figure 17 GF height corresponding the minimum power for the 1/rev motion.

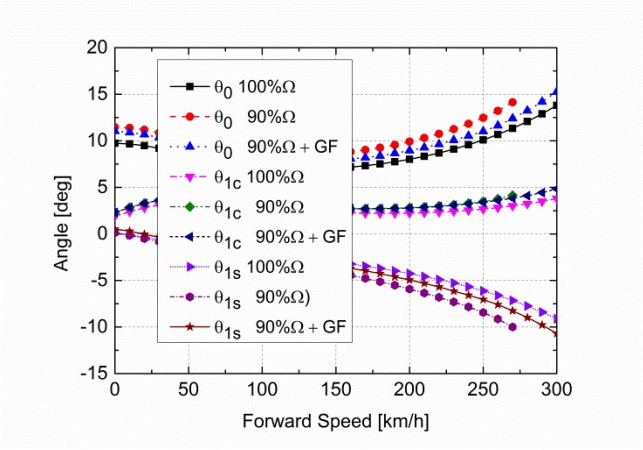

Figure 18 The collective, longitudinal and lateral cyclic pitches for the 1/rev GF.

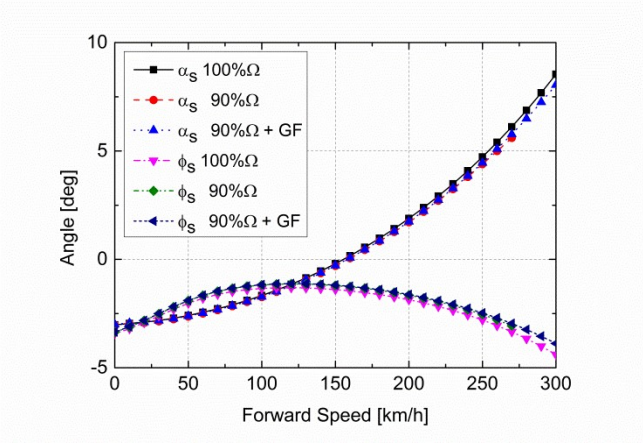

Figure 19 The longitudinal and lateral tilts of rotor shaft for the 1/rev GF.

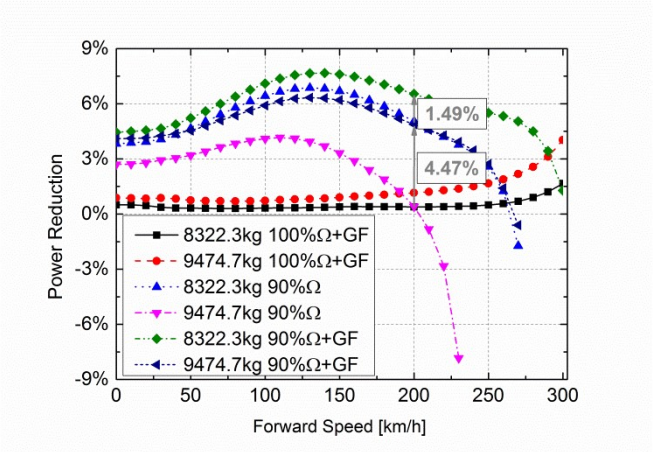

Figure 20 Power reduction for larger take-off weight.

Figure 20 shows the power reductions for different take-off weights. With larger weight, the GF can achieve much more power savings, especially at high speed flight. At a weight of 8322.3 kg and rotor speed of 90%Ω, the 1/rev GF can yield 1.49% more power reduction than without GF. As the weight changes to 9474.7 kg (weight coefficient 0.0074 at 100%Ω), this value becomes 4.47%. It is obvious that the GF can achieve better performance improvement in high thrust cases, and the maximum forward speed can be increased. To attain larger maximum forward speeds, the rotor speed can be reduced to decrease the blade tip Mach number in the advancing side, and the 1/rev GF could be used to alleviate stall in the retreating side. This may be a practical way to achieve higher speed for high speed helicopters.

4.2 2/rev

For different forward speeds, the influence of the phase of the 2/rev retractable GF on the power is shown in Figure 21. The magnitude A is set to 2%c. At low to medium forward speed, the power changes little with the phase. At high speed flight, the variation of the power with the phase is clear. The best phase for the minimum power is around 110°. In the following analyses, this could be used.

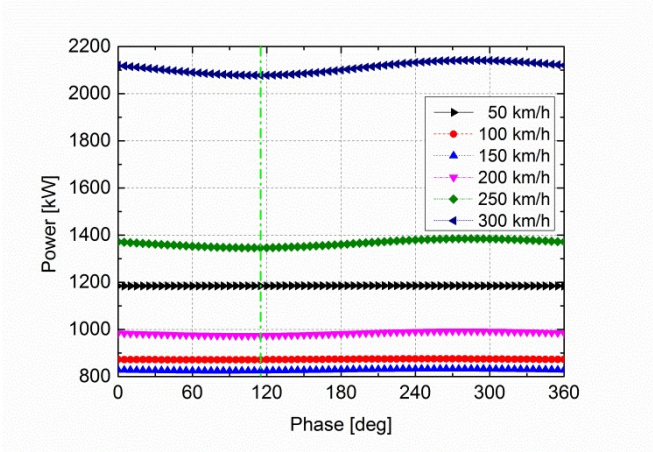

Figure 21 Power with 2/rev GF motion.

Figure 22 shows the power reduction for different forward and rotor speeds. The power is the minimum for a GF with $h \leq 5\%c$. Compared to the 1/rev, the 2/rev GF results in smaller power reduction. At a speed of 300 km/h and rotor speed of 100%Ω, the 1/rev GF obtains 3.51% power reduction, and this value is 2.18% for the 2/rev GF. At a rotor speed of 85%Ω, the maximum power reduction with the 1/rev GF is 10.7%, and this value is 10.2%. From the point of view of power reduction , a lower harmonic GF is preferred.

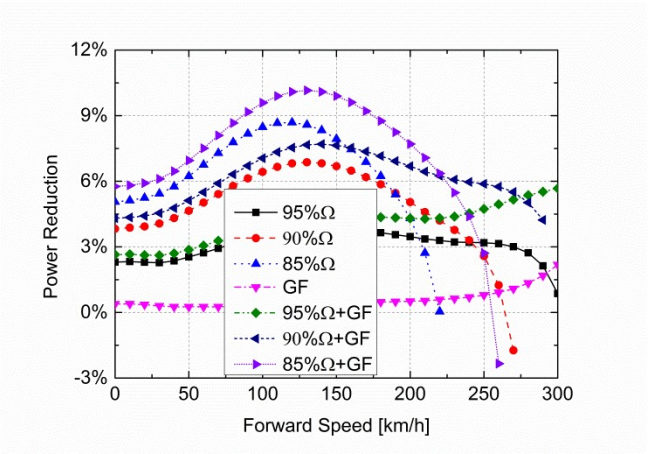

Figure 22 Power reduction for the 2/rev motion.

Figure 23 shows the height of the 2/rev GF corresponding to the minimum rotor power. With increasing forward speed, the GF height first decreases slightly and then increases. The trend changes smoothly at low to medium speed. At high speed flight, the required height increases dramatically. Lowering the rotor speed, larger height is needed. At high speed fight, a height larger than 2.5%c is needed, which is due to the height limit set in this study. If a larger height is available, a larger power reduction in high speed flight can be obtained. At a speed of 200 km/h, the average heights for the 100%Ω, 95%Ω, 90%Ω, and 80%Ω are 0.4%c, 0.6%c, 0.9%c and 1.2%c. For the 1/rev GF, the average heights change to 0.6%c, 0.8%c, 1.1%c and 1.7%c, respectively. It is obvious that for larger harmonic motion, a smaller height is better.

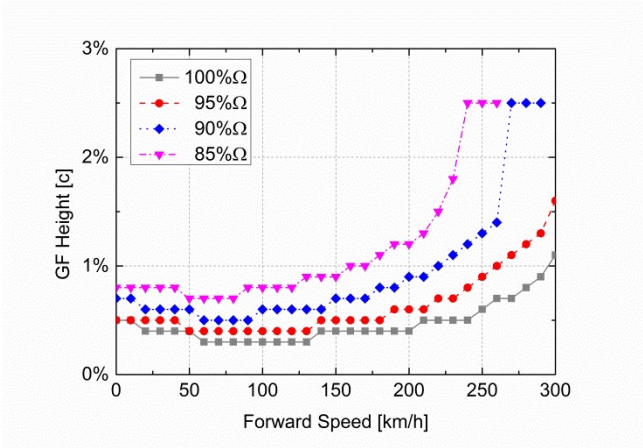

Figure 23 GF height corresponding the minimum power for the 2/rev motion.

4.3 Higher Harmonic GF

Figure 24 shows the power reduction for different harmonics of the GF at a weight of 8322.3 kg and rotor speed of 100%Ω. The average height is fixed at 2%c, and the phase is shifted to the value corresponding to the minimum power at the prescribed speed. It is clear that the power savings decrease with increasing harmonics. **The higher harmonic input requires GFs of multiply height. For a rotor, a larger height of the GF is needed in or around the stall region at the retreating side due to the higher efficiency of GF in high lift. In other regions, larger heights of the GF give additional drag penalties corresponding to higher power consumption. It is natural that the higher harmonic saves less power.** A 2%c GF is the larger value investigated. At high speed flight, power savings can also be obtained. For the 1-4/rev GF, the power reductions at a speed of 300 km/h are 3.51%, 1.71%, 0.765% and 0.557%, respectively. It is obvious that the 1/rev harmonic motion gives the best performance improvement. The saving is also larger than the power saved by the fixed height GF shown in Figure 9. **From the point of view of blade loads, usually the 1/rev load is the dominant component. It is then possible to simultaneously reduce the rotor power, and decrease the blade loads using the 1/rev GF.**

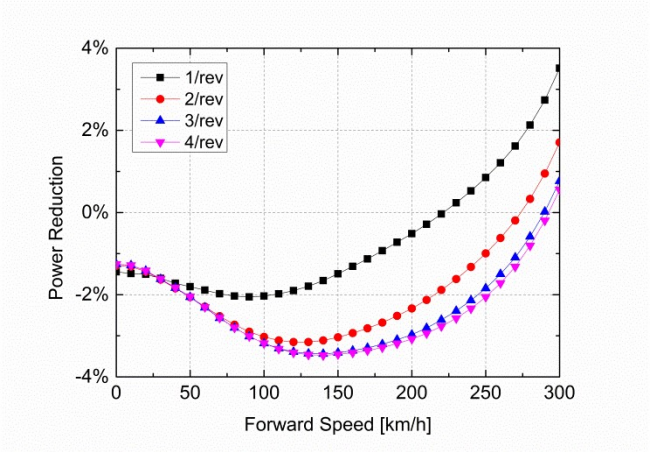

Figure 24 Higher harmonic input.

5. Conclusions

An empirical helicopter model was used to explore performance improvement of variable speed rotors by GFs. The flight data of the UH-60A helicopter was used to validate the model. The predictions of the rotor power were in good agreement with the flight test data, justifying the application of the present method in analyzing rotor performance. The analyses yielded the following conclusions:

1) The GF with fixed height can enhance the performance of variable speed rotors and expand the corresponding flight envelop, especially near stall, and at high speed flight. At lower rotor speeds, more rotor power can be saved. The flap height corresponding to the maximum power reduction, decreases slightly with forward speed and then increases. At high speed flight, the power reduction increases dramatically with the flap height.

2) The 1/rev retractable GF can yield more power savings than a fixed one. At a speed of 200km/h, the 1/rev GF obtained 3.22% more power reduction at a rotor speed of 85%Ω. This value was 8.37% at 220km/h. The flap height corresponding to the minimum power increases slowly at low to medium flight speed, and increases much higher at high speed flight.

3) The 1/rev GF can obtain more rotor power savings for larger weights.

4) The 2/rev retractable GF gives smaller power savings than the 1/rev GF at the same fight condition. The average height is also smaller than for the 1/rev GF.

5) The power reduction decreases with the increase of the GF harmonics. The 1/rev GF can obtain the maximum

power savings, and it is also larger than the fixed height GF.

6) The deployment of the GF decreases the collective pitch by a small amount. The changes to the cyclic pitches and tilt of rotor shaft are relatively small.

It should be noted that practical application of Gurney flaps may also have side effects, such as increase in the weight and system complexity, extra power consumption required to drive the Gurney flaps, and so on.

Finally, it is noted that the precise numbers given above are specific to the blade utilized in this work. For a rotor with different planform, airfoils, diameter, etc., the optimum deployment and performance improvement levels may vary.

Conflict of Interest Statement

There is no conflict of interest.

Acknowledgments

This work is supported from the National Natural Science Foundation of China (11472129), the Aeronautical Science Foundation of China (20165752048), and Science and Technology on Rotorcraft Aeromechanics Laboratory Foundation (6142220050416220002).

References

1. Prouty, R. W., “Should We Consider Variable Rotor Speeds? ” Vertiflite, Vol. 50, No. 4, 2004, pp. 24-27.
2. Steiner, J., Gandhi, F., and Yoshizaki, Y., “An Investigation of Variable Rotor RPM on Performance and Trim,” the American Helicopter Society 64th Annual Forum, Montreal, Canada, April 29-May 1, 2008.
3. Horn, J. F., and Guo, W., “Flight Control Design for Rotorcraft with Variable Rotor Speed,” American Helicopter Society 64th Annual Forum Proceedings, Montreal, Canada, April 29 - May 1, 2008.
4. Guo, W., and Horn, J. F., “Helicopter Flight Control with Variable Rotor Speed and Torque Limiting,” American Helicopter Society 65th Annual Forum Proceedings, Grapevine, TX, May 27-29, 2009.
5. DiOttavio, J., and Friedmann, D., “Operational Benefit of an Optimal, Widely Variable Speed Rotor,” the American Helicopter Society 66th Annual Forum, Phoenix, AZ, May 11-13, 2010.
6. Mistry, M., and Gandhi, F., “Helicopter Performance Improvement with Variable Rotor Radius and RPM,” Journal of the American Helicopter Society, Vol. 59, No. 4, 2014, pp. 17-35.
7. Misté, G. A., Benini, E., Garavello, A., and Gonzalez-Alcoy, M., “A Methodology for Determining the Optimal Rotational Speed of a Variable RPM Main Rotor/Turboshaft Engine System,” Journal of the American Helicopter Society, Vol. 60, No. 3, 2015, pp. 0320091-03200911.
8. Bowen-Davies, G. M., and Chopra, I., “Aeromechanics of a Slowed Rotor,” Journal of the American Helicopter Society, Vol. 60, No. 3, 2015, pp. 0320111-03201113.
9. Han, D., Pastrikakis, V., and Barakos, G. N., “Helicopter Performance Improvement by Variable Rotor Speed and Variable Blade Twist,” Aerospace Science and Technology, Vol. 54, 2016, pp.164-173.
10. Kang H, Saberi H, and Grandhi F., “Dynamic blade shape for improved helicopter rotor performance,” Journal of the American Helicopter Society, Vol.55, No. 3, 2010, pp. 0320081-03200811.
11. Wang, J. J., Li, Y. C., Choi, K.-S., “Gurney Flap - Lift Enhancement, Mechanisms and Applications,” Progress in Aerospace Sciences, Vol. 44, No. 1, 2008, pp. 22-47.
12. Palacios, J., Kinzel, M., and Overmeyer, A, “Active Gurney Flaps: Their Application in a Rotor Blade Centrifugal Field,” Journal of Aircraft, Vol. 51, No. 2, 2014, pp. 473-489.

13. Kentfield, J. A. C., “The Potential of Gurney Flaps for Improving the Aerodynamic Performance of Helicopter Rotors,” AIAA Paper 1993-4883, AIAA International Power Lift Conference, Santa Clara, CA, December 1-3, 1993.
14. Kinzel, M. P., Maughmer, M. D., and Lesieutre, G. A., “Miniature Trailing-Edge Effectors for Rotorcraft Performance Enhancement,” Journal of the American Helicopter Society, Vol. 52, No, 2, 2007, pp. 146-158.
15. Pastrikakis, V. A., Steijl, R., Barakos G. N., and Małecki, J., “Computational Aeroelastic Analysis of a Hovering W3 Sokol Blade with Gurney Flap,” Journal of Fluids and Structures, Vol. 53, 2015, pp. 96-111.
16. Pastrikakis, V. A., Steijl, R., and Barakos G. N., “Effect of Active Gurney Flaps on Overall Helicopter Flight Envelope,” The Aeronautical Journal, Vol. 120, No. 1230, 2016, pp. 1230-1261.
17. Min, B.-Y., Sankar, L. N., Rajmohan, N., and Prasad, “Computational Investigation of Gurney Flap Effects on Rotors in Forward Flight,” Journal of Aircraft, Vol. 46, No. 6, 2009, pp. 1957-1964.
18. Liu, L., Padthe, A. K., and Friedmann, P. P., “Computational Study of Microflaps with Application to vibration Reduction in Helicopter Rotors,” AIAA Journal, Vol. 49, No. 7, 2011, pp. 1450-1465.
19. Min, B.-Y., Sankar, L. N., and Bauchau, O. A., “A CFD-CSD Coupled-Analysis of HART II Rotor Vibration Reduction Using Gurney Flaps,” Aerospace Science and Technology, Vol. 48, 2016, pp. 308-321.
20. Peters, D.A. and HaQuang N., “Dynamic Inflow for Practical Application,” Journal of the American Helicopter Society, Vol. 33, No. 4, 1988, pp. 64-68.
21. Leishman, J. G., Principles of Helicopter Aerodynamics, 2nd ed., Cambridge University Press, New York, USA, 2006, pp. 202-209.
22. Yeo, H., Bousman, W. G. and Johnson, W., “Performance Analysis of a Utility Helicopter with Standard and Advanced Rotors,” Journal of the American Helicopter Society, Vol. 49, No. 3, 2004, pp. 250-270.
23. Cheng, R. P., Theodore, C. R., and Celi, R., “Effects of Two/rev Higher Harmonic Control on Rotor Performance,,” Journal of the American Helicopter Society, Vol. 48, No. 1, 2003, pp. 18-27.
24. Cheng, R. P., and Celi, R., “Optimum Two-Per-Revolution Inputs for Improved Rotor Performance,” Journal of Aircraft, Vol. 42, No. 6, 2005, pp. 1409-1417.
25. Hilbert, K. B., “A Mathematical Model of the UH-60 Helicopter,” Technical Report NASA-TM-85890, 1984.
26. DavisS. J., “Pedesign Study for a Modern 4-Bladed Rotor for the RSRA,” Technical Report NASA-CR-166155, 1981.
27. Buckanin, R. M., Herbst, M. K., Lockwood, R. A., Skinner, G. L. and Sullivan, P. J., “Airworthiness and Flight Characteristics Test of a Sixth Year Production UH-60A,” Final Report, USAAEFA Project No. 83-24, June1985.
28. Nagata, J. I., Piotrowski, J. L., Young, C. J., Lewis, W. D., Losier, P. W. and Lyle, J. A., “Baseline Performance Verification of the 12th Year Production UH-60A Black Hawk Helicopter,” Final Report, USAAEFA Project No. 87-32, January 1989.
29. Han, D., Pastrikakis, V. and Barakos, G., “Helicopter Performance Improvement by Dynamic Blade Twist,” Aerospace Science and Technology, Vol. 58, 2016, pp. 445-452.
30. Li, Y., Wang, J., and Zhang, P., “Effects of Gurney Flaps on a NACA0012 Airfoil,” Flow, Turbulence and Combustion, Vol. 68, No. 1, 2002, pp. 27-39.
31. Bowen-Davies, G. M., and Chopra, I., “Aeromechanics of a Slowed Rotor,” Journal of the American Helicopter Society, Vol. 60, No. 3, 2015, pp. 032011.